

Most precise single redshift bound to $\Delta\alpha/\alpha^*$

S. A. Levshakov¹, M. Centurión², P. Molaro^{2,3}, S. D’Odorico⁴,
D. Reimers⁵, R. Quast⁵, and M. Pollmann⁵

¹ Department of Theoretical Astrophysics, Ioffe Physico-Technical Institute, 194021 St.Petersburg, Russia

² Osservatorio Astronomico di Trieste, Via G. B. Tiepolo 11, 34131 Trieste, Italy

³ Observatoire de Paris 61, avenue de l’Observatoire, 75014 Paris, France

⁴ European Southern Observatory, Karl-Schwarzschild-Strasse 2, D-85748 Garching bei München, Germany

⁵ Hamburger Sternwarte, Universität Hamburg, Gojenbergsweg 112, D-21029 Hamburg, Germany

Received 00 / Accepted 00

Abstract. Verification of theoretical predictions of an oscillating behavior of the fine-structure constant α ($\equiv e^2/\hbar c$) with cosmic time requires high precision $\Delta\alpha/\alpha$ measurements at individual redshifts, while in earlier studies the mean $\Delta\alpha/\alpha$ values averaged over wide redshift intervals were usually reported. This requirement can be met via the single ion differential α measurement (SIDAM) procedure proposed in Levshakov et al. (2005). We apply the SIDAM to the Fe II lines associated with the damped Ly α system observed at $z_{\text{abs}} = 1.15$ in the spectrum of HE 0515–4414. The weighted mean $\langle\Delta\alpha/\alpha\rangle$ calculated on base of carefully selected 34 Fe II pairs $\{\lambda 1608, X\}$ ($X = 2344, 2374$, and 2586 Å) is $\langle\Delta\alpha/\alpha\rangle = (-0.07 \pm 0.84) \times 10^{-6}$ (1σ C.L.). The precision of this estimate improves by a factor 2 the previous one reported for the same system by Quast et al. (2004). The obtained result represents an absolute improvement with respect to what has been done in the measurements of $\Delta\alpha/\alpha$.

Key words. Cosmology: observations – Line: profiles – Quasars: absorption lines – Quasars: individual: HE 0515–4414

1. Introduction

One of the most important physical constants, the Sommerfeld fine-structure constant α , is subjected to more and more precise measurements in both modern laboratory experiments and astronomical observations due to fundamental rôle which α plays in quantum electrodynamics effects and in electromagnetic and optical properties of atoms. An unprecedented accuracy of $\sim 0.1 \times 10^{-9}$ (the relative error) has been recently achieved in the laboratory measurements of the atomic transitions in alkali atoms (Banerjee et al. 2004). This result, combined with sub-ppb (parts per billion) measurements of the atomic masses (Bradley et al. 1999), enables a high-precision determination of the fine-structure constant at the present time, i.e. at the cosmological epoch $z = 0$.

The question whether or not the value of α varied at different cosmological epochs can be answered only through spectral studies of extragalactic objects. Theoretically the effects of inhomogeneous space and time

evolution of α were considered by Marciano (1984) and Mota & Barrow (2004). Most recently Fujii & Mizuno (2005) and Fujii (2005) suggested a damped-oscillation-like behavior of α as a function of cosmic time t . It is apparent that to study such irregular changes in α , we need to achieve high precision in the measurements of $\Delta\alpha/\alpha$ at *individual* redshifts, contrary to the averaging procedure over many redshifts which is usually used to decrease uncertainties of the mean values $\langle\Delta\alpha/\alpha\rangle$ (see, e.g., Murphy et al. 2004, and references therein).

Contemporary astronomical observations still cannot provide accuracy comparable to the laboratory results. Up to now, the errors of the fractional deviation of the fine-structure constant, $\Delta\alpha/\alpha = (\alpha_z - \alpha_0)/\alpha_0$, recovered from astronomical spectra are at the level of 10^{-6} (or parts per million, ppm)¹. For instance, individual $\Delta\alpha/\alpha$ values obtained by Chand et al. (2004) are known with the accuracy of a few ppm. The uncertainty of the same order of magnitude, $\sigma_{\langle\Delta\alpha/\alpha\rangle} \simeq 1.7\text{--}1.9$ ppm, was achieved in our previous study of the $z_{\text{abs}} = 1.15$ system towards HE 0515–4414 (Quast et al. 2004, hereafter QRL). In both cases the standard many-multiplet (MM) method (Webb et al. 1999;

Send offprint requests to: S. A. Levshakov
lev@astro.ioffe.rssi.ru

* Based on observations performed at the VLT Kueyen telescope (ESO, Paranal, Chile). The data are retrieved from the ESO/ST-ECF Science Archive Facility.

¹ Here α_0 and α_z denote the values of the fine-structure constant at epoch $z = 0$ and in a given absorption (or emission) line system at redshift z , respectively.

Table 1. ESO UVES archive data on the quasar HE 0515–4414

Exp. No.	Set- ting (1)	Slit, arcsec (2)	Date, y-m-d (4)	Time, h:m (5)	Exposure, h:m (6)	Seeing, \mathcal{S} , arcsec (7)	T, °C (8)	P, mb (9)	Quality, κ (10)	Programme ID (11)
1b	346	0.8	1999-12-14	05:27	1:15	0.46–0.56	11.8–12.8	990.4–991.0	0.2	60.A-9022
1r	580	0.7		05:27						
2b	346	0.8	1999-12-14	06:43	1:15	0.56–1.04	11.5–11.9	990.1–990.3	0.3	60.A-9022
2r	580	0.7		06:43						
3b	346	0.8	1999-12-15	04:47	1:30	0.51–1.84	10.1–11.9	990.0–990.8	0.006	60.A-9022
3r	580	0.7		04:47						
4b	346	0.8	2000-11-17	06:42	1:15	0.34–0.53	13.5–13.8	990.1–990.3	1.0	66.A-0212
4r	580	0.8		06:42						
5b	346	0.8	2000-11-18	07:25	1:15	0.55–0.85	13.2–13.7	989.1–989.2	0.8	66.A-0212
5r	580	0.8		07:25						
6b	346	0.8	2000-11-19	07:27	1:15	0.58–0.80	13.2–14.0	989.2–989.5	0.2	66.A-0212
6r	580	0.8		07:27						
7b	346	0.8	2000-12-25	06:13	1:15	0.55–0.88	15.8–16.5	989.9–990.0	0.5	66.A-0212
7r	580	0.8		06:13						

Seeing, \mathcal{S} , temperature, T , and air pressure, P , limiting values listed, respectively, in Cols.7, 8 and 9 are taken from the ESO/ST-ECF Science Archive Ambient Conditions Database at <http://archive.eso.org/>

Dzuba et al. 1999, 2002) has been used. Further modification of the MM method (Levshakov 2004; Levshakov et al. 2005, hereafter LCMD) resulted in a new methodology for probing the cosmological variability of α on base of pairs of Fe II lines observed in *individual exposures* from a high resolution spectrograph (henceforth referred to as SIDAM – single ion differential α measurement). The basic idea behind SIDAM was to avoid the influence of small spectral shifts due to ionization inhomogeneities within the absorbers and due to non-zero offsets between different exposures. The individual offsets can affect the shape of the line profiles during rebinning and coadding procedures which are usually applied to combine exposures together to increase signal-to-noise, S/N, ratio (examples are given in LCMD).

In the present paper we show that the SIDAM can provide a sub-ppm precision in a single redshift $\Delta\alpha/\alpha$ measurement and that this level of accuracy is caused by *intrinsic instrumental imperfections* and *systematic errors* inherited from the uncertainties of the wavelength scale calibration.

While working at sub-ppm level, we confront the problem of *sub-pixel* centering. As shown by David & Verschueren (1995), this problem can be properly treated only in two cases: either (i) the exact analytical function describing the observed line profile is known a priori, or (ii) the observed line profile is intrinsically symmetric. Neither of these conditions is fulfilled for metal absorption lines observed in QSO spectra. This means that in general the line centering must be handled with special care. We discuss this problem in detail in Sects. 2 and 3. The results of the SIDAM are presented in Sect. 4. Our conclusions are given in Sect. 5.

Table 2. ESO UVES archive data on ThAr lamp used to calibrate spectra of HE 0515–4414

ThAr No.	Date, y-m-d	Time, h:m	T, °C	P, mb
1	1999-12-14	08:17	11.8	990.0
4	2000-11-17	07:58	13.7	990.1
5	2000-11-18	08:41	13.3	989.1
6	2000-11-19	08:44	14.1	989.3
7	2000-12-25	07:29	16.5	990.0

Temperature and air pressure are taken from the ESO/ST-ECF Science Archive Ambient Conditions Database at <http://archive.eso.org/>

2. Observations and Data Reduction

We analyze high quality spectra of the bright intermediate redshift quasar HE 0515–4414 ($z_{\text{em}} = 1.73$, $B = 15.0$; Reimers et al. 1998). The observations were acquired with the UV-Visual Echelle Spectrograph (UVES) at the VLT 8.2 m telescope at Paranal, Chile, and the spectral data were retrieved from the ESO archive. The selected exposures are listed in Table 1. The spectra were recorded with a dichroic filter which allows to work with the blue and red UVES arms simultaneously as with two independent spectrographs, and the CCDs were read-out in 1×1 binned pixels (spatial \times dispersion direction). The standard settings at central wavelengths $\lambda 346$ nm and $\lambda 580$ nm were used for the blue and red arms respectively (marked by symbols ‘b’ and ‘r’ in Col.1 of Table 1 (along with the exposure number)). From the blue spectra we used only order

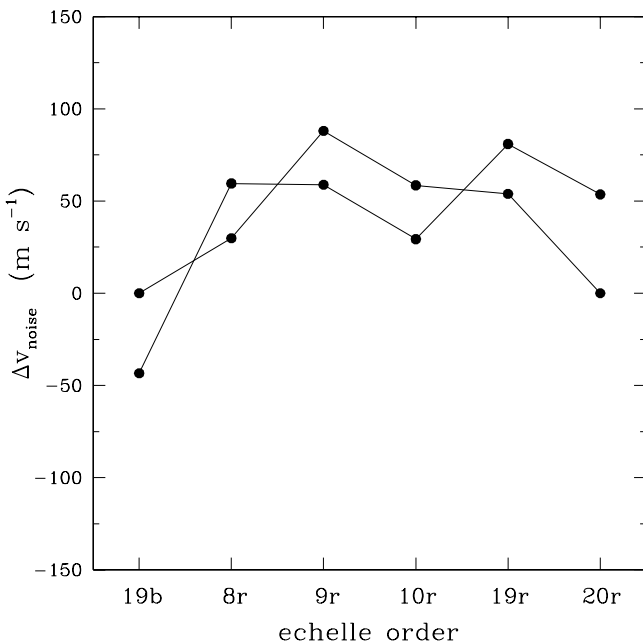


Fig. 1. Doppler shifts of two calibrated ThAr lines bracketing the positions of the Fe II absorption complex (Fig. 2) for exposure No.1 (Table 2). Echelle orders (Table 3) are indicated on the bottom axis ('b' and 'r' denote the blue and red arms, respectively). The ThAr lines used are the following (wavelengths in Å): 3457.070 & 3462.851 (19b), 5039.230 & 5041.122 (8r), 5101.129 & 5111.278 (9r), 5122.499 & 5125.489 (10r), 5559.891 & 5564.201 (19r), and 5595.063 & 5599.654 (20r). The peak-to-peak variations of $\Delta v_{\text{noise}} \sim 100 \text{ m s}^{-1}$ set a lower limit to the error of the Fe II relative position measurements

19, and from the red spectra orders 8, 9, 10, 19 and 20², where Fe II lines suitable for the $\Delta\alpha/\alpha$ measurement are observed. All selected Fe II lines are located close to the central regions of the corresponding echelle orders. This minimizes possible distortions of the line profiles caused by the decreasing spectral sensitivity at the edges of echelle orders (LCMD).

Other details of the observations are also presented in Table 1. Cols. 2 and 3 give setting and slit width used. Cols. 4 and 5 list the date and the starting time of the exposure whose duration is indicated in Col. 6. The ambient conditions are characterized by minimum and maximum values of the seeing, S , temperature, T , and air pressure, P (Cols.7-9). During an integration these quantities were varying between the indicated limits. Col. 11 shows that the data were obtained for two observational programs, 60.A-9022 and 66.A-0212. To characterize the quality of the obtained spectra, we introduce a quality factor, κ (Col. 10), defined as $\kappa = 1/(\Delta S \cdot \Delta T \cdot \Delta P)$ and

² These are the sequential numbers of the echelle orders which are used throughout the paper. The correspondence between them and echelle orders is as follows: 19b=135, 8r=121, 9r=120, 10r=119, 19r=110, and 20r=109.

Table 3. Original pixel sizes along the selected echelle orders

Echelle order	$\Delta\lambda (\text{\AA})$ Pixel size (m\AA)	$\lambda(\text{Fe II})$ complex (\AA) Pixel size (km s ⁻¹)
blue arm	3449–3469	3459
#19	19.5–16.0	1.55
red arm	5030–5050	5040
#8	22.7–20.5	1.29
red arm	5095–5115	5104
#9	20.4–17.9	1.13
red arm	5113–5133	5123
#10	23.2–21.0	1.30
red arm	5552–5572	5562
#19	22.9–20.5	1.17
red arm	5581–5601	5591
#20	25.3–23.2	1.30

expressed in fractions of the 4th exposure which has the highest quality. The selection of variables ΔS , ΔT , and ΔP is heuristic in some sense but it is relevant to the problem of the line centering. For instance, a change of $\Delta P = 1$ millibar (or a change of $\Delta T = 0.3^\circ\text{C}$) induces an error in radial velocities of $\sim 50 \text{ m s}^{-1}$ (Kaufer, D'Odorico & Kaper 2004). Problems may also occur because of seeing variations which change the intensity of the QSO signal during an integration, and, hence, the instabilities of the spectrograph may be sampled in different ways. Other effects like vibration, thermal drift, changes of the grating spacing due to temperature fluctuations, unequal illumination of the spectrograph grating and collimator by the laboratory reference source and starlight, varying width of the instrumental profile, and scattered light may produce additional Doppler noise at the level of a few m s^{-1} (Griffen & Griffen 1973; Brown 1990; Meyer 1990; Gulliver et al. 1996). These deleterious effects do not permit very precise measurements of the line positions even from extremely high S/N spectra. However, these problems can be considerably reduced using fiber fed spectrographs like, e.g., a configuration of UVES+FLAMES which provides the radial velocity precision better than 100 m s^{-1} for the stars with V magnitudes in the range 14–18 (Melo et al. 2004; Bouchy et al. 2005).

We used the UVES pipeline (the routines implemented in MIDAS-ESO data reduction package for UVES data) to perform the bias correction, inter-order background subtraction, flat-fielding, correction of cosmic rays impacts, sky subtraction, extraction of the orders in the pixel space and wavelength calibration. A modified version of the routine 'echred' of the context ECHELLE inside MIDAS was used to calibrate in wavelength the echelle spectra *without rebinning*. In this way we have the reduced spectra with their original pixel size in wavelength.

The residuals of the calibrations are rather small amounting to $\sigma_{\text{rms}} \lesssim 1 \text{ m\AA}$. The observed wavelength

Table 4. The instrumental profile widths (FWHM) in km s^{-1} and the mean signal-to-noise ratios per pixel (given in parentheses) at the continuum level at the positions of Fe II lines in scientific exposures

Echelle order	Scientific exposures						
	#1	#2	#3	#4	#5	#6	#7
19b	$5.60_{-0.10}^{+0.10}(31)$	$5.60_{-0.10}^{+0.10}(31)$	$5.60_{-0.10}^{+0.10}(27)$	$5.60_{-0.10}^{+0.10}(31)$	$5.60_{-0.10}^{+0.10}(31)$	$5.60_{-0.10}^{+0.10}(28)$	$5.60_{-0.10}^{+0.10}(35)$
8r	$4.88_{-0.07}^{+0.07}(46)$	$4.88_{-0.07}^{+0.07}(50)$	$4.88_{-0.07}^{+0.07}(43)$	$5.50_{-0.10}^{+0.10}(56)$	$5.40_{-0.10}^{+0.10}(54)$	$5.50_{-0.20}^{+0.20}(51)$	$5.50_{-0.06}^{+0.06}(51)$
9r	$4.77_{-0.05}^{+0.05}(51)$	$4.77_{-0.05}^{+0.05}(57)$	$4.77_{-0.05}^{+0.05}(49)$	$5.36_{-0.09}^{+0.09}(44)$	$5.43_{-0.08}^{+0.08}(47)$	$5.47_{-0.08}^{+0.08}(52)$	$5.47_{-0.08}^{+0.08}(45)$
10r	$4.84_{-0.09}^{+0.09}(47)$	$4.84_{-0.09}^{+0.09}(43)$	$4.84_{-0.09}^{+0.09}(42)$	$5.46_{-0.12}^{+0.12}(49)$	$5.46_{-0.12}^{+0.12}(52)$	$5.54_{-0.11}^{+0.11}(50)$	$5.46_{-0.05}^{+0.05}(53)$
19r	$4.78_{-0.03}^{+0.03}(47)$	$4.78_{-0.03}^{+0.03}(54)$	$4.78_{-0.03}^{+0.03}(49)$	$5.39_{-0.11}^{+0.11}(53)$	$5.45_{-0.32}^{+0.32}(54)$	$5.61_{-0.27}^{+0.27}(59)$	$5.45_{-0.11}^{+0.11}(54)$
20r	$4.83_{-0.05}^{+0.05}(53)$	$4.83_{-0.05}^{+0.05}(49)$	$4.83_{-0.05}^{+0.05}(45)$	$5.42_{-0.05}^{+0.05}(44)$	$5.47_{-0.11}^{+0.11}(60)$	$5.53_{-0.11}^{+0.11}(55)$	$5.42_{-0.05}^{+0.05}(48)$

scale of each spectrum was transformed into vacuum, heliocentric wavelength scale (Edlén 1966).

Following the same procedure as for the QSO exposures, we calibrated in wavelength the spectra of the ThAr arcs. This allowed us to estimate the ‘Doppler noise’ by measuring the random velocity shifts of the ThAr emission lines. For each order we selected two well-exposed ThAr emissions which bracket the positions of the Fe II absorption complex. In Fig. 1 we show the Doppler shifts, Δv_{noise} , measured with the calibrated ThAr lamp No.1 (Table 2). For both lines of the arc the peak-to-peak variations of Δv_{noise} are about 100 m s^{-1} . This gives us a lower limit to the error of Fe II positional estimations.

Usually when a precise absolute wavelength scale is required, calibration exposures are taken before and after the scientific exposures. As discussed above, varying ambient weather conditions may introduce different velocity offsets in the lamp and QSO spectra if they were not obtained closely in time. However, this uncertainty affects only an absolute calibration whereas in $\Delta\alpha/\alpha$ estimations we are dealing with *differential* measurements. In fact, we measure the relative Fe II positions with respect to the Fe II $\lambda 1608$ line (LCMD). Since the SIDAM uses iron lines obtained simultaneously in one exposure, a systematic offset caused by shortcomings of the calibration procedure should be canceled out for the blue and red arms spectra. This is not the case if unexpected mechanical instabilities occur during integration (see Sect. 3 below and an example in LCMD where effects of the mechanical instabilities are discussed). For our data, the first three QSO exposures were calibrated with the same ThAr lamp No.1 (Table 2). The 4th to 7th QSO exposures were calibrated with the corresponding ThAr lamps No.4-7 taken immediately after the scientific exposures (cf. Tables 1 and 2).

Our further concern was nonlinearity of the wavelength scale. Off-plane design in echelle spectrographs like UVES is introducing a pronounced curvature of the orders (e.g. Ballester & Rosa 1997). As a result, the wavelength scale is not linear in the sense that the original pixel width in wavelength decreases with increasing pixel number along the frame. Table 3 illustrates this behavior for the selected echelle orders. In Col.2, upper row for each echelle order

indicates the wavelength range which includes the Fe II absorptions, whereas the corresponding pixel sizes at the starting and end points of this range are given below. Col.3 shows the pixel size at the center position of the Fe II complex (lower and upper rows, respectively). The Fe II complex is depicted in Fig. 2.

The difference between pixel sizes at the edges of the wavelength ranges shown in Fig. 2 and Table 3 is about 18% for order 19 (blue arm) and 8-12% for the red arm orders. This introduces an artificial inclination of the local continuum level which may affect the relative positions of the Fe II lines at the sub-pixel level. Therefore we normalized the registered photocounts per pixel to the original pixel size in wavelength and determined the local continua for each Fe II complex following linear regression procedure from LCMD. The uncertainties of the calculated continua are less than 1% in all Fe II regions. An example of the continuum fitting is shown in Fig. 2 for the 4th QSO exposure.

Finally, we measured the FWHM of the instrumental profile for each individual echelle order. The instrumental profile is dominated in our case by the slit width which was different for the blue and red arms in the first three exposures (Table 1). The FWHM values calculated from the narrow lines of the arc spectra are given in Table 4. Our further results were obtained with the mean FWHM and signal-to-noise ratio values listed in Table 4.

3. Concordance of the Fe II profiles

The spectra of HE 0515-4414 reveal a multi-component complex of metal absorption lines associated with a sub-damped Ly α (sub-DLA) system at $z_{\text{abs}} = 1.15$ (de la Varga et al. 2000; Quast et al. 2002; Reimers et al. 2003). The radial velocities of the absorption components of the Fe II complex span 660 km s^{-1} (QRL, Table 2). Not all of them are seen, however, in the individual exposures, the weakest ones were detected only in the co-added spectra (QRL, Fig. 1). Therefore, for our purpose we chose two sub-systems at $z_{\text{abs}} = 1.150965$ and 1.149092 which exhibit the most pronounced absorption features and, thus, provide the most accurate determination of their relative positions from individual exposures. The atomic data used for the analysis are given in Table 5.

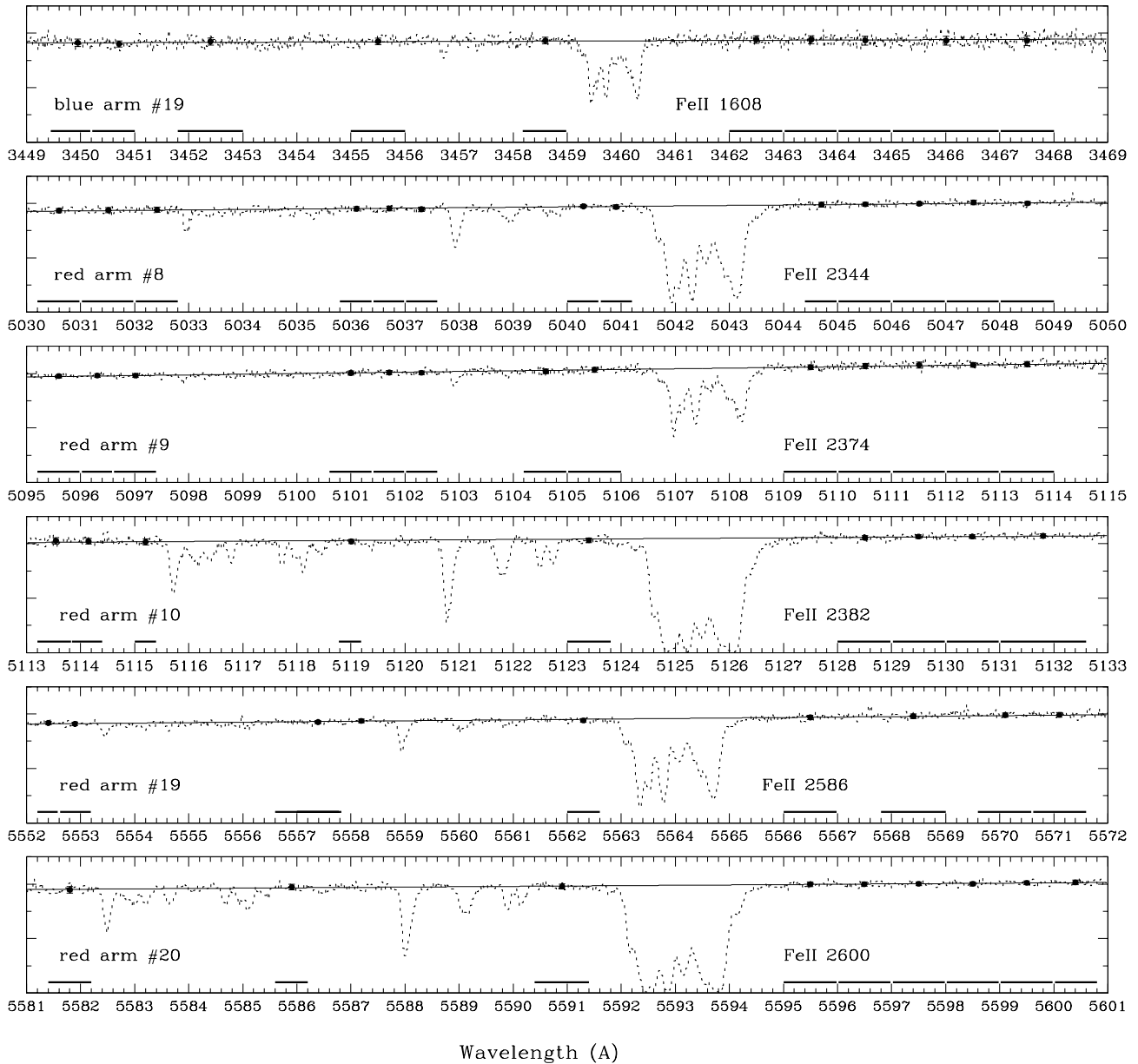


Fig. 2. Unnormalized portions of the HE 0515-4414 spectra (intensities are in arbitrary units) with the Fe II lines ($z_{\text{abs}} = 1.15$) obtained from the 4th exposure (Table 1). All Fe II lines are located near the center of the orders (indicated at the left side of each panel). Dots with error bars are the mean intensities and their 1σ errors (calculated in the ranges marked with horizontal lines) used to estimate the local continua by means of the linear regression analysis (LCMD). The uncertainty of each local continuum level is less than 1%

In both sub-systems there are no isolated and symmetric absorption components which could be used for the line centering. But, as explained in LCMD, we are mainly interested in the position of an absorption complex as a whole to calculate its radial velocity shift with respect to the reference line Fe II $\lambda 1608$ – the only line among Fe II transitions which has a negative sensitivity coefficient Q (Table 5).

In general, the position of the line blend is sensitive to the relative strengths of the partly resolved and unresolved (hidden) components as well as to the shape of the instrumental profile. The effect is most noticeable in

the case of optically thick and narrow hidden components due to their different saturation depending on the line strength (Levshakov 1994; Levshakov & D'Odorico 1995; QRL). As seen from Table 5, the strengths of the iron lines, $\log f\lambda_{\text{vac}}$, most frequently observed in QSO spectra (Fe II $\lambda\lambda 2374, 2382$) differ by an order of magnitude.

To handle the blend we have to adopt a specific model. Since we are dealing with only one ion, all Fe II lines from an intervening absorber *must* have similar profiles. A model not matching all observational profiles simultaneously either indicates blended lines from different intervening systems or that some data points are outliers. This

Table 5. Atomic data of the Fe II transitions^a, and the sensitivity coefficients Q^b . Estimated errors are given in parentheses

Mlt. No. ^c	λ_{vac} , Å	f	Q	$\log f \lambda_{\text{vac}}$
1u	2600.1725(1)	0.23878	0.035(4)	2.79
1u	2586.6496(1)	0.06918	0.039(4)	2.25
2u	2382.7642(1)	0.320	0.035(4)	2.88
2u	2374.4603(1)	0.0313	0.038(4)	1.87
3u	2344.2130(1)	0.114	0.028(4)	2.43
8u	1608.45080(8)	0.0580	-0.021(5)	1.97

^abased on the compilation of Murphy et al. (2003);

^bdefined in Sect. 4; ^cmultiplet numbers from Morton (2003)

allows us to check concordance of the Fe II data before evaluating $\Delta\alpha/\alpha$.

To define the model we will assume, following LCMD, that: (1) the number of subcomponents n_s is fixed for all Fe II lines under study; (2) the Doppler b_i parameters are identical for the same i th subcomponents; (3) the relative intensities of the subcomponents $r_{i,j}$ and (4) the relative radial velocities $\delta v_{i,j}$ between the subcomponents are fixed.

Then, an Fe II blend can be described by the sum of n_s Voigt functions:

$$\tau_v^{(\ell)} = N_1 \sum_{i=1}^{n_s} r_{i,1} \mathcal{V}[(v - v_\ell - \delta v_{i,1})/b_i], \quad (1)$$

where $\tau_v^{(\ell)}$ is the optical depth at radial velocity v within the ℓ th Fe II line ($\ell = 1, 2, \dots, L$), N_1 is the column density of the main component, $r_{i,1} = N_i/N_1$, v_ℓ is the position of the main component in the line ℓ , and $\delta v_{1,1} = 0$. Here L is the total number of Fe II lines involved in the analysis.

The model is fully defined by specifying $p = 3n_s + L - 1$ parameters: N_1 , $\{b_i\}_{i=1}^{n_s}$, $\{\Delta v_{i,1}\}_{i=1}^{n_s-1}$, $\{r_{i,1}\}_{i=1}^{n_s-1}$, and $\{v_\ell\}_{\ell=1}^L$. All these parameters are components of the parameter vector $\theta = \{\theta_1, \theta_2, \dots, \theta_p\}$. To estimate θ from the combined Fe II profiles, we minimize the objective function

$$\chi^2(\theta) = \frac{1}{\nu} \sum_{\ell=1}^L \sum_{j=1}^{m_\ell} [\mathcal{F}_{\ell,j}^{\text{cal}}(\theta) - \mathcal{F}_{\ell,j}^{\text{obs}}]^2 / \sigma_{\ell,j}^2, \quad (2)$$

where $\mathcal{F}_{\ell,j}^{\text{obs}}$ is the observed normalized intensity of the spectral line ℓ , $\sigma_{\ell,j}$ is the experimental error within the j th pixel of the line profile, and $\nu = \sum_\ell^L m_\ell - p \equiv M - p$ is the number of degrees of freedom. $\mathcal{F}_{\ell,j}^{\text{cal}}(\theta)$ is the calculated intensity convolved with the corresponding spectrograph point-spread function (Table 4).

The total number of data points involved in the analysis is $M = 2704$ ($z_{\text{abs}} = 1.150965$) and $M = 428$ ($z_{\text{abs}} = 1.149092$). All selected Fe II profiles are free from cosmic rays and telluric absorptions. In accord with QRL, we took $n_s = 8$ ($p = 65$) and $n_s = 2$ ($p = 47$) to define our models for the former and the latter sub-systems. We found that the models chosen described both sets of data adequately:

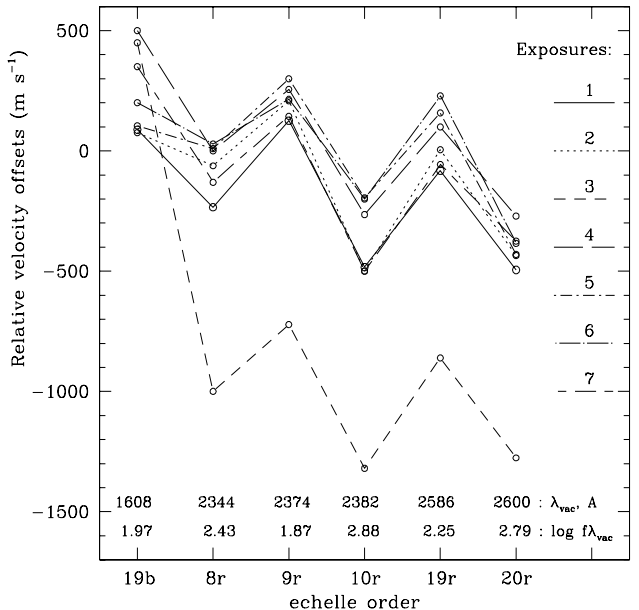


Fig. 3. Same as Fig. 1 but for the Fe II lines from the $z_{\text{abs}} = 1.150965$ system. The exposure numbering is given in accord with Table 1, whereas the line strengths and wavelengths – according to Table 5. The relative velocity offsets are based on the 8-component model estimations (see text for details)

the χ^2_ν per degree of freedom was about 1 in both cases. Thus, each ensemble of Fe II lines is self-consistent, free from outliers and blending with other lines.

This preliminary analysis revealed, however, an unexpectedly large shift between the blue and red arms for the 3rd exposure (short-dashed line in Fig. 3). It might be a chance coincidence, but the spectral data obtained from the 3rd exposure have the lowest quality factor $\kappa = 0.006$ as compared with unity (see Table 1). The quality factors for other exposures are much larger and do not exhibit significant variations in their values. Similar offsets between the blue and red arms were noted for the UVES spectra of Q 1101–264 in LCMD where we ascribed them to mechanical instabilities. Such exposures were excluded from further $\Delta\alpha/\alpha$ measurements since they may induce a mock signal.

Fig. 3 shows one more problem: there are too large peak-to-peak variations of the relative velocity offsets, Δv , and we note a clear dependence of Δv on the line strength. This behavior can be corrected by excluding saturated lines (like Fe II $\lambda 2382$ and $\lambda 2600$) from the analysis, and by increasing the number of sub-components to account for the influence of the unresolved (hidden) blends on the line centering. The number of sub-components is controlled by two factors: (i) the value of χ^2_{min} should be close to unity, while (ii) the dispersion of Δv should decrease but not differ much from that deduced from ThAr lines shown in Fig. 1. Fig. 4 (upper panel) shows the results obtained for a model with $n_s = 13$ sub-components ($p = 62$).

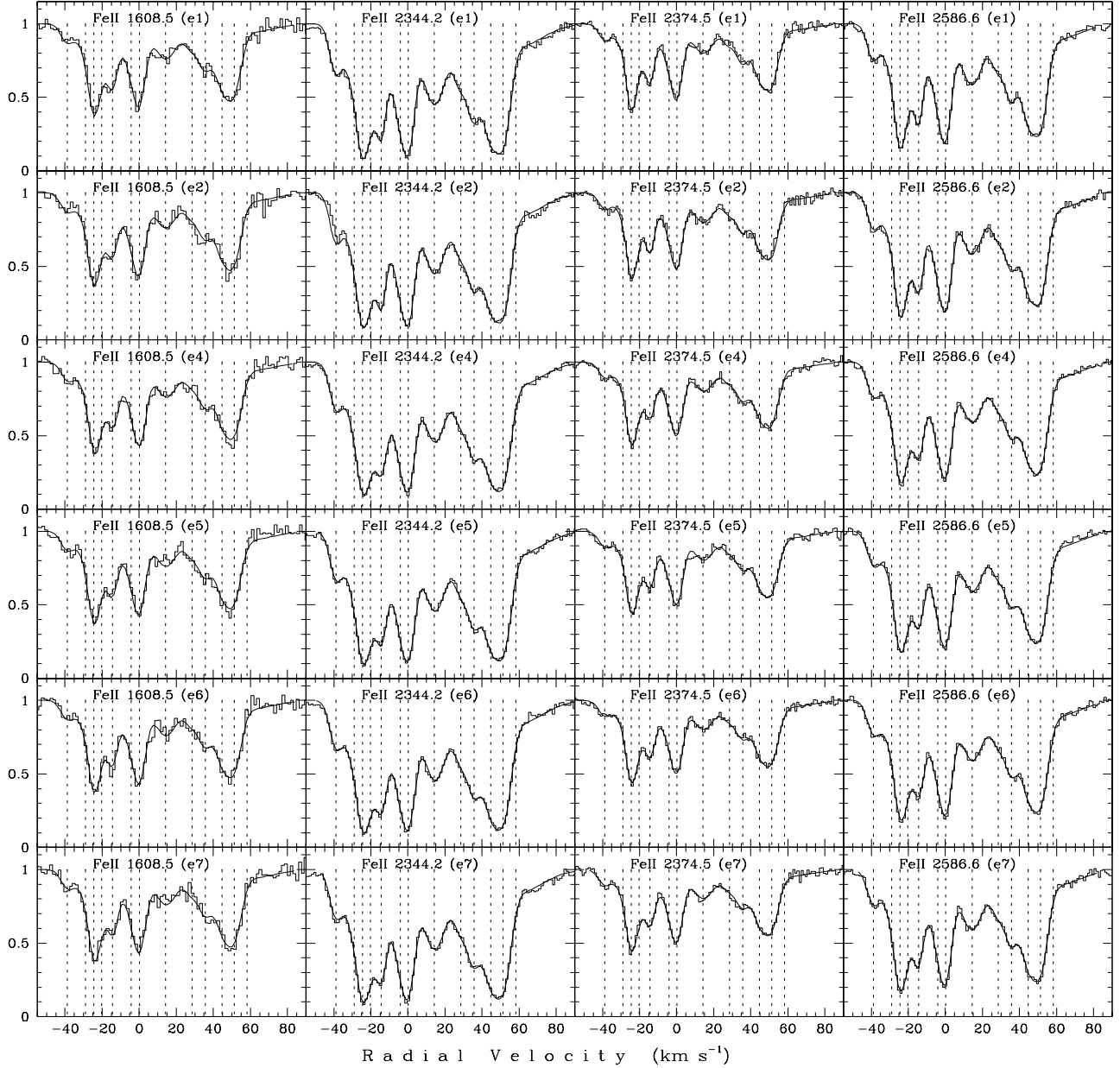


Fig. 5. Individual exposures (labeled as ‘e#’) of the Fe II lines selected from the spectrum of HE 0515–4414 to estimate $\Delta\alpha/\alpha$. Normalized intensities are indicated by histograms. The over-potted synthetic profiles (smooth curves) are calculated from the joint analysis of all iron lines. The zero radial velocity is fixed at $z = 1.150965$. The minimization procedure gives $\chi^2_{\min} = 0.9$ per degree of freedom ($\nu = 2642$). The dashed vertical lines mark positions of the sub-components from Table 6

The estimation of the uncertainties of the best-fitting model parameters in case of many-dimensional parameter space requires a special approach. When $p \gg 1$, the parameters are as a rule correlated, the parameter space near the minimum of the objective function has a complicated topology and the $\Delta\chi^2$ levels for the confidence regions cannot be accurately defined. In such cases Monte Carlo simulations are recommended instead of the formal inversion of the covariance matrix (see, e.g., Press et al. 1989, Chapter 15). We used the bootstrapping residuals method to estimate the standard error (σ_{rms}) of the

best-fitting parameters. The trial datasets are created in the following way. Suppose $\tilde{\theta}$ is the estimated parameter vector and $r_{\ell,j} = \mathcal{F}_{\ell,j}^{\text{cal}} - \mathcal{F}_{\ell,j}^{\text{obs}}$ are the residuals. Then a new dataset $\mathcal{F}_{\ell,j}^{\text{obs}*}$ is made by sampling independently from $r_{\ell,j}$ for each line ℓ , yielding $r_{\ell,j}^*$, and by setting $\mathcal{F}_{\ell,j}^{\text{obs}*} = \mathcal{F}_{\ell,j}^{\text{cal}}(\tilde{\theta}) + r_{\ell,j}^*$. New values $\tilde{\theta}^*$ of the parameter vector are then computed from the bootstrap data in the same way that $\tilde{\theta}$ was computed from the original data, i.e., by least squares.

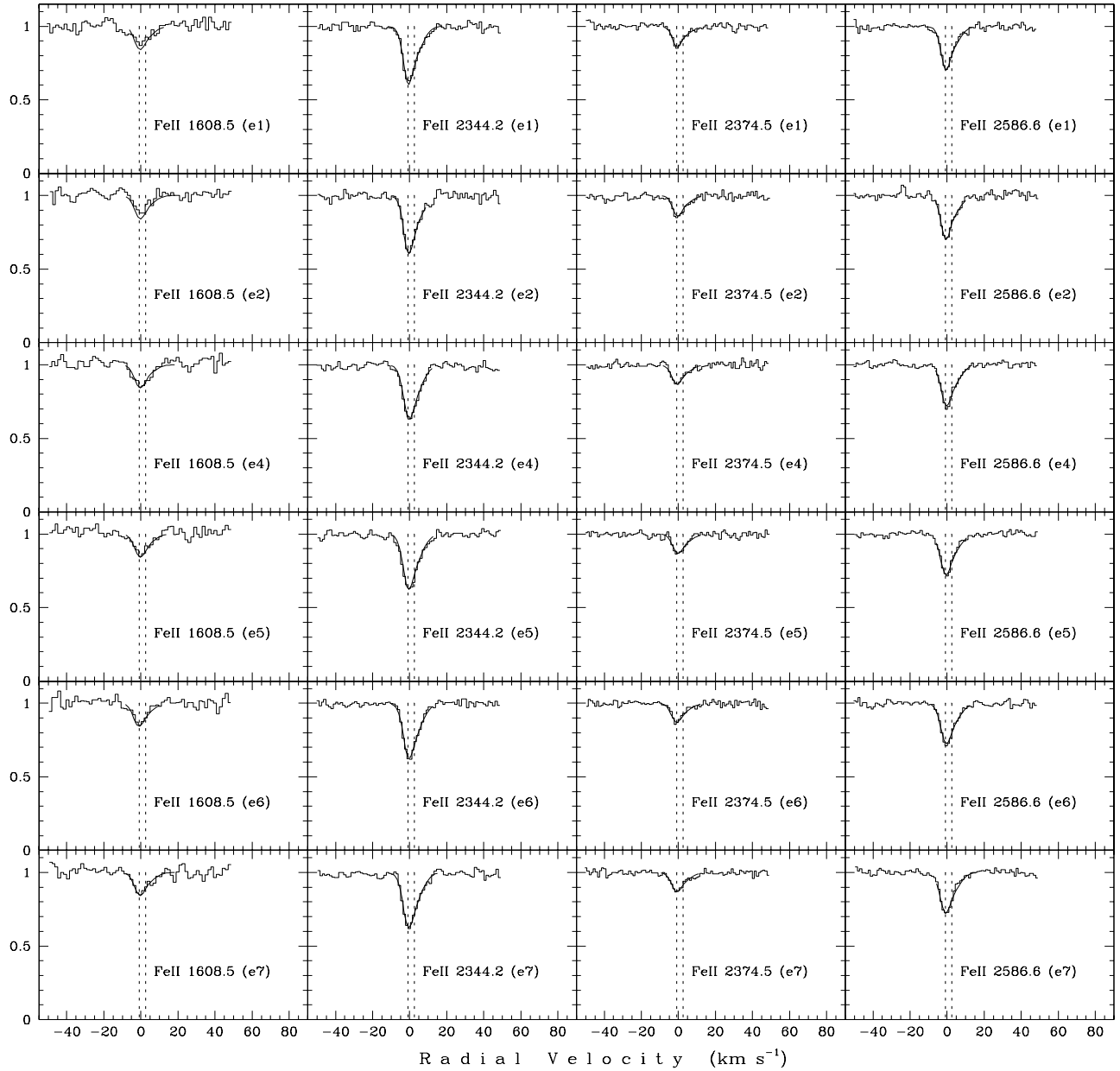


Fig. 6. Same as Fig. 5 but for the sub-system at $z_{\text{abs}} = 1.149092$. The minimization procedure gives $\chi^2_{\text{min}} = 0.8$ per degree of freedom ($\nu = 399$). The dashed vertical lines mark positions of the sub-components from Table 7

The model parameters and their uncertainties computed on the base of 30 bootstrap samples are given in Table 6. The peak-to-peak variations are now diminished by a factor of 2-3 and are equal to 200 m s^{-1} in average.

The lower panel in Fig. 4 shows the peak-to-peak variations for the second sub-system with $z_{\text{abs}} = 1.149092$. A larger dispersion of Δv in this case (peak-to-peak variations $\simeq 300 \text{ m s}^{-1}$, except the 6th exposure) is a consequence of the lower accuracy of the line centering because of considerably smaller equivalent widths of the Fe II lines. Table 7 lists the model parameters for the second Fe II ensemble where $n_s = 2$ ($p = 29$).

Fig. 5 ($z_{\text{abs}} = 1.150965$) and Fig. 6 ($z_{\text{abs}} = 1.149092$) show the synthetic profiles (smooth curves) with corre-

sponding QSO data (normalized intensities) plotted by histograms. The positions of the sub-components are marked by vertical dotted lines. The corresponding χ^2_{min} values are 0.9 ($\nu = 2642$) and 0.8 ($\nu = 399$) for the former and the latter sub-systems, respectively.

4. $\Delta\alpha/\alpha$ measurements

The relativistic corrections of the Fe II transition frequencies to the changes in α (the so-called q -coefficients) have been calculated by Dzuba et al. (2002). In our analysis we use the dimensionless sensitivity coefficients, $\mathcal{Q} \equiv q/\omega_0$, listed in Table 5 (here $\omega_0 = 1/\lambda_0$ is the laboratory wavenumber). Then, the value of $\Delta\alpha/\alpha$ can be estimated

Table 6. SIDAM analysis: relative positions of the Fe II lines (with respect to the adopted redshift of 1.150965), δv , the line broadening velocities, b , the column densities, $\log N$, and the corresponding rms errors (given in parentheses) of the 13 components constituting the Fe II absorption complex at $z_{\text{abs}} = 1.151$

Fe II line (Å)	Positions of the main subcomponent in different exposures, v (km s $^{-1}$)					
	#1	#2	#4	#5	#6	#7
1608	0.536(0.086)	0.511(0.085)	0.907(0.086)	0.582(0.085)	0.636(0.086)	0.810(0.087)
2344	0.533(0.076)	0.688(0.076)	0.790(0.077)	0.804(0.077)	0.804(0.077)	0.645(0.077)
2374	0.562(0.087)	0.656(0.084)	0.719(0.086)	0.729(0.083)	0.667(0.085)	0.609(0.085)
2586	0.498(0.080)	0.618(0.080)	0.679(0.080)	0.739(0.080)	0.813(0.080)	0.544(0.079)
Model parameters						
Component No.	δv , km s $^{-1}$		b , km s $^{-1}$		$\log N$, cm $^{-2}$	
1	0.000		2.55(0.13)		13.243(0.049)	
2	-39.23(0.10)		3.71(0.08)		12.701(0.080)	
3	-30.02(0.67)		4.07(0.76)		12.790(0.079)	
4	-24.96(0.19)		2.31(0.09)		13.458(0.075)	
5	-20.56(0.40)		2.01(0.33)		12.859(0.099)	
6	-14.95(0.17)		2.33(0.17)		13.245(0.081)	
7	-3.85(0.37)		5.05(0.15)		13.268(0.111)	
8	13.74(0.09)		7.33(0.12)		13.205(0.068)	
9	28.46(0.37)		4.69(0.49)		12.893(0.111)	
10	35.23(0.14)		3.03(0.31)		12.987(0.102)	
11	44.04(0.20)		4.35(0.25)		13.287(0.078)	
12	50.68(0.14)		3.96(0.10)		13.313(0.080)	
13	58.12(1.22)		18.53(0.93)		12.913(0.054)	

Table 7. Same as Table 6 but for the Fe II absorption complex at $z_{\text{abs}} = 1.149092$ (the two component model)

Fe II line (Å)	Positions of the main subcomponent in different exposures, v (km s $^{-1}$)					
	#1	#2	#4	#5	#6	#7
1608	-0.821(0.557)	-0.988(0.572)	-0.854(0.413)	-0.695(0.376)	-1.457(0.319)	-1.010(0.226)
2344	-0.989(0.112)	-0.867(0.096)	-0.739(0.104)	-0.978(0.160)	-0.762(0.121)	-0.914(0.152)
2374	-0.902(0.109)	-0.713(0.245)	-1.014(0.212)	-0.595(0.198)	-1.325(0.255)	-1.165(0.119)
2586	-0.928(0.088)	-1.017(0.069)	-0.683(0.183)	-1.068(0.167)	-0.828(0.106)	-1.245(0.106)
Model parameters						
Component No.	δv , km s $^{-1}$		b , km s $^{-1}$		$\log N$, cm $^{-2}$	
1	0.000		1.51(0.01)		12.501(0.002)	
2	3.39(0.02)		5.60(0.01)		12.536(0.002)	

from a pair of lines with different sensitivity coefficients. In linear approximation ($|\Delta\alpha/\alpha| \ll 1$), eq.(5) from LCMD can be re-written in the form:

$$\frac{\Delta\alpha}{\alpha} = \frac{(v_2 - v_1)}{2c(Q_1 - Q_2)}, \quad (3)$$

where the line positions v_1 and v_2 are taken from the same exposure. Here index ‘1’ is assigned to the line $\lambda 1608$, while index ‘2’ marks one of the other Fe II lines ($\lambda 2344$, $\lambda 2374$, or $\lambda 2586$). The calculated $\Delta\alpha/\alpha$ values are given in Table 8 along with their rms errors estimated by the standard method of error propagation.

We now have everything we need to compute statistics: the mean value $\langle \Delta\alpha/\alpha \rangle$ and its error. We note that for each individual exposure the uncertainty of $\Delta\alpha/\alpha$ is dominated by the error of the line centering of the ‘blue’ Fe II $\lambda 1608$ line since its strength is smaller as compared with the ‘red’ lines and the Fe II $\lambda 1608$ spectra have systematically lower S/N. Our approach reveals also a systematic effect for all the exposures except the first one for the subsystem $z_{\text{abs}} = 1.150965$: the individual values of $\Delta\alpha/\alpha$ have the same sign. At $z_{\text{abs}} = 1.149092$, the sign of $\Delta\alpha/\alpha$ does not vary in the 1st and 6th exposures, whereas different signs are observed in the 4th, 5th, and 7th exposures. However, being combined the whole sample provides

Table 8. SIDAM analysis: $\Delta\alpha/\alpha$ (ppm) calculated with eq.(3) and their σ_{rms} errors (given in parentheses)

Exp. No.	Fe II pairs		
	1608/2344	1608/2374	1608/2586
$z_{\text{abs}} = 1.150965$			
1	0.07(3.92)	-0.73(3.45)	1.03(3.27)
2	-6.05(3.90)	-4.12(3.38)	-2.97(3.26)
4	3.99(3.93)	5.32(3.44)	6.34(3.26)
5	-7.57(3.90)	-4.17(3.37)	-4.36(3.24)
6	-5.74(3.92)	-0.88(3.41)	-4.93(3.26)
7	5.61(3.95)	5.68(3.42)	7.39(3.27)
$z_{\text{abs}} = 1.149092$			
1	5.69(19.34)	2.28(16.05)	2.95(15.68)
2	-4.12(19.74)	-7.77(17.59)	0.83(16.02)
4	-3.93(14.51)	4.51(13.14)	-4.76(12.57)
5	9.64(13.91)	-2.84(12.02)	10.37(11.44)
6	-23.57(11.61)	-3.73(11.54)	-17.47(9.34)
7	-3.27(9.27)	4.40(7.23)	6.55(6.95)

19 negative and 17 positive $\Delta\alpha/\alpha$ values which randomize these systematic shifts. Moreover, from inspecting the data listed in Table 8, one finds that two values -23.569 and -17.466 from the 6th exposure ($z_{\text{abs}} = 1.149092$) are sharply distinct from the others and exceed $3\sigma_{\text{rms}}$ from the weighted mean. These measurements were rejected from the further analysis. Thus the final ensemble consists of the equal number ($n = 17$) of negative and positive $\Delta\alpha/\alpha$ values.

For the weights, w_i , we use σ_{rms}^{-2} values from Table 8. The unbiased estimators of the weighted mean $\tilde{x} = \langle \Delta\alpha/\alpha \rangle$, and the variance of \tilde{x} are the quantities (Linnik 1961):

$$\tilde{x} = \frac{[wx]}{[w]}, \quad (4)$$

and

$$\text{Var}(\tilde{x}) = \frac{[w \tilde{a} \tilde{a}]}{(n-1)[w]}, \quad (5)$$

where $\tilde{a} = x_i - \tilde{x}$ are ‘apparent errors’, and square brackets denote summation, e.g., $[w] = \sum_{i=1}^n w_i$, $[wx] = \sum_{i=1}^n w_i x_i$.

We find that the weighted mean of the ensemble of $n = 34$ $\Delta\alpha/\alpha$ values and the accuracy of its determination are equal to $\langle \Delta\alpha/\alpha \rangle = -0.07 \pm 0.84$ ppm (1σ C.L.).

5. Discussion and Conclusions

We re-analyzed the profiles of the Fe II lines associated with the sub-DLA system observed at $z_{\text{abs}} = 1.15$ in the spectrum of HE 0515–4414. Our main purpose was to achieve the highest possible accuracy in the line centering to set the most stringent constraint at a single redshift to the hypothetical variability of the fine-structure constant.

This work was inspired by our recent results (LCMD) showing the influence of reduction errors and instabilities in the instrument on the relative radial velocity shifts

in the merged QSO spectra. It was demonstrated that co-added spectra, minded to enhance the signal-to-noise ratio, may affect the shapes of narrow absorption lines because each calibrated exposure has its own velocity offset.

In the previous estimations of $\Delta\alpha/\alpha$ from the co-added spectrum of HE 0515–4414 (QRL), we found that in spite of a good fit of the 8-component model of the Fe II profiles to the high S/N data, the normalized residuals showed an unexpected pattern in their radial velocity distribution (see Fig. 7, upper panel). It was suggested that this pattern may be caused by the presence of unresolved narrow lines (or non-Gaussian line profiles) which may induce some kind of correlations between the residuals. We now recognize that additional correlations may be due to zero-point errors as well.

If individual scientific exposures are treated separately and the number of the model components is increased up to 13, the pattern is vanished and the residuals become uncorrelated (see Fig. 7, lower panel). This demonstrates a clear advantage of the differential measurements. Moreover, the precision of the new estimate of $\langle \Delta\alpha/\alpha \rangle$ is improved by a factor of 2. From a general point of view, such an improvement would require 4 times longer total exposure time under the same observational conditions (i.e., 36h vs 9h, in our case).

In this respect, the present work indicates that all steps in the data reduction procedure and in the long-term stability of the instrument must be of a particular concern while dealing with sub-pixel positional measurements with echelle spectrographs. To make full and accurate utilization of the information derived from the observations a detailed knowledge of the instrumental characteristics is required.

In the present analysis, we have reached an accuracy in the line centering which is comparable to the accuracy of the wavelength scale calibration, $\sigma_{\text{rms}} \sim 1$ mÅ. From eq.(3) it follows that this value corresponds to the sys-

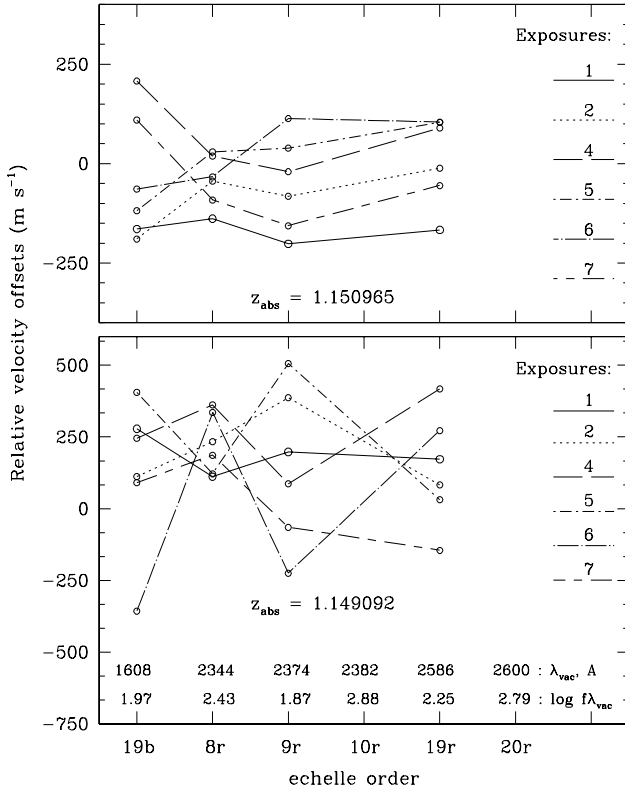


Fig. 4. Same as Fig. 3 but for the Fe II lines from the $z_{\text{abs}} = 1.150965$ and $z_{\text{abs}} = 1.149092$ systems. The corresponding models are superpositions of $n_s = 13$ and $n_s = 2$ Voigt profiles. The upper panel illustrates the effect of hidden (unresolved) components: the peak-to-peak variations of Δv are decreasing with increasing number of sub-components. Smaller equivalent widths of the Fe II lines at $z_{\text{abs}} = 1.149092$ lead to a larger dispersion of the Δv values shown in the lower panel

tematic error of the individual determination of $\Delta\alpha/\alpha$ of $\sigma_{\text{sys}} \sim 4$ ppm (calculated from a pair of Fe II lines with $|\Delta Q| = 0.06$). This adds a systematic error of about 1 ppm to the total error budget of the weighted mean, $\sigma_{\text{tot}}^2 = \sigma_{\langle\Delta\alpha/\alpha\rangle}^2 + \sigma_{\text{sys}}^2 \simeq 1.19$ ppm².

It should be emphasized that the level of $\langle\Delta\alpha/\alpha\rangle = (-5.7 \pm 1.1)$ ppm found by Murphy et al. (2004) was estimated from a large sample of 143 absorption systems ranging from $z = 0.2$ to 4.2 which were observed with the HIRES/Keck spectrograph (here the error of the mean includes only statistical uncertainties). Since for the individual system at $z = 1.15$ the accuracy of $\langle\Delta\alpha/\alpha\rangle$ is better than 1 ppm, we are now in the position of arguing if the Keck ensemble average is biased.

We notice that the level of $\Delta\alpha/\alpha$ expected at $z = 1.15$ from the damped-oscillatory model by Fujii (2005) is 2 ppm (see Fig. 8). We do not see this value in our analysis. However, the total error of $\langle\Delta\alpha/\alpha\rangle$ is not small enough to verify or reject Fujii's model. With the probability level of 0.05 we cannot take the observed difference between -0.07 ppm and 2 ppm as significant according to the t -

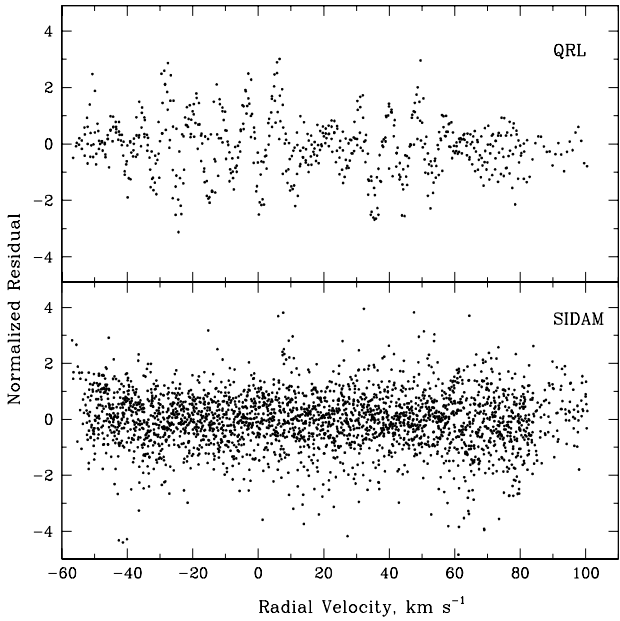


Fig. 7. The normalized residuals, $(\mathcal{F}^{\text{cal}} - \mathcal{F}^{\text{obs}})/\sigma$, for the Fe II profiles ($\lambda\lambda 1608, 2344, 2374$, and 2586 Å) calculated from the 8-component model in QRL (upper panel) and from the 13-component model in the present work (lower panel). The zero radial velocity is fixed at $z = 1.150965$

test. To probe the oscillatory behavior of α , very accurate measurements of $\Delta\alpha/\alpha$ at higher redshifts (where the amplitude of $\Delta\alpha/\alpha$ is expected to be ± 5 ppm) are required.

As a conclusion, it is worthwhile to note that the achieved accuracy of $\Delta\alpha/\alpha$ is unique for the standard UVES configuration and that further improvement at the sub-ppm level can be attained only with increasing spectral resolution and stabilizing instrumental performance such as, for instance, a fiber link producing a stable illumination at the entrance of the spectrograph and allowing continuous simultaneous comparison spectrum.

Acknowledgements. S.A.L. gratefully acknowledges the hospitality of Hamburger Sternwarte where this work was completed. This research has been supported by the RFBR Grant No. 03-02-17522 and by the RLSS Grant No. 1115.2003.2, and by the Deutsche Forschungsgemeinschaft under Grant No. Re 353/48-1.

References

- Ballester, P., & Rosa, M. R. 1997, A&AS, 126, 563
- Banerjee, A., Das, D., & Natarajan, V. 2004, Europhys. Lett., 65, 172
- Bouchy, F., Pont, F., Melo, C., Santos, N. C., Mayor, M., Queloz, D., & Udry, S. 2005, A&A, 431, 1105
- Bradley, M. P., Porto, J. V., Rainville, S., Thompson, J. K., & Pritchard, D. E. 1999, Phys. Rev. Lett., 83, 4510
- Brown, T. M. 1990, in CCDs in Astronomy, ed. G. H. Jacoby, PASPC 8, 335
- Chand, H., Srianand, R., Petitjean, P., & Aracil, B. 2004, A&A, 417, 853

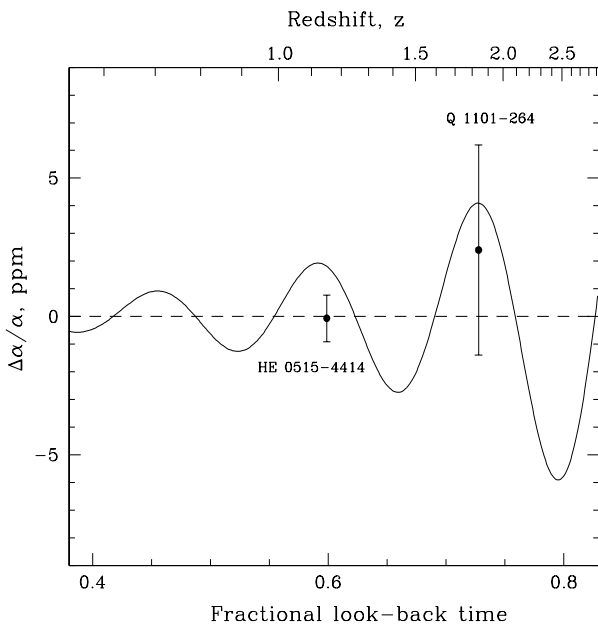


Fig. 8. The curve illustrating an oscillatory behavior of $\Delta\alpha/\alpha$ as a function of time is taken from the middle panel of Fig. 1 in Fujii (2005). The SIDAM results shown by dots with 1σ error bars (indicated are statistical errors) are from the $z_{\text{abs}}=1.15$ system towards HE 0515-4414 (present work) and from the $z_{\text{abs}}=1.839$ system towards Q 1101-264 (LCMD). The fractional look-back time is calculated with the cosmological parameters $h = 0.7$, $\Omega_M = 0.3$, and $\Omega_\Lambda = 0.7$

David, M., & Verschueren, W. 1995, A&AS, 111, 183
 de la Varga, A., Reimers, D., Tytler, D., Barlow, T., & Burles, S. 2000, A&A, 363, 69
 Dzuba, V. A., Flambaum, V. V., Kozlov, M. G., & Marchenko, M. V. 2002, Phys. Rev. A, 66, 022501
 Dzuba, V. A., Flambaum, V. V., & Webb, J. K. 1999, Phys. Rev. A, 59, 230
 Edlén, B. 1966, Metrologia, 2, 71
 Fujii, Y. 2005, Phys. Lett. B, 616, 141
 Fujii, Y., & Mizuno, S. 2005, Int. J. Mod. Phys. D, 14, 677
 Griffin, R., & Griffin, R. 1973, MNRAS, 162, 243
 Gulliver, A. F., Hill, G., & Adelman, S. J. 1996, in Model Atmospheres and Spectrum Synthesis, eds. S. J. Adelman, F. Kupka, and W. W. Weiss, ASP Conf. Ser. 108, 232
 Kaufer, A., D'Odorico, S., & Kaper, L. 2004. UV-Visual Echelle Spectrograph. User Manual (<http://www.eso.org/instruments/uves/userman/>), p. 40
 Levshakov, S. A., Centurión, M., Molaro, P., & D'Odorico, S. 2005, A&A, 434, 827 [LCMD]
 Levshakov, S. A. 2004, in Astrophysics, Clocks and Fundamental Constants, eds. S. G. Karshenboim and E. Peik (Springer-Verlag: Berlin, Heidelberg), p.151
 Levshakov, S. A., & D'Odorico, S. 1995, in QSO Absorption Lines, ed. G. Meylan, p.202
 Levshakov, S. A. 1994, MNRAS, 269, 339
 Linnik, Yu. V. 1961, Method of Least Squares and Principles of the Theory of Observations (Pergamon Press: NY)
 Marciano, W. J. 1984, Phys. Rev. Lett., 52, 489

Melo, C., Bouchy, F., Pont, F., Santos, N. C., Mayor, M., Queloz, D., & Udry, S. 2004, The Messenger, 116, 32
 Meyer, D. M. 1990, in CCDs in Astronomy, ed. G. H. Jacoby, PASPC, 8, 345
 Morton, D. C. 2003, ApJS, 149, 205
 Mota, D. F., & Barrow, J. D. 2004, MNRAS, 349, 291
 Murphy, M. T., Flambaum, V. V., Webb, J. K., Dzuba, V. V., Prochaska, J. X., & Wolfe, A. M. 2004, in Astrophysics, Clocks and Fundamental Constants, eds. S. G. Karshenboim and E. Peik (Springer-Verlag: Berlin, Heidelberg), p.131
 Murphy, M. T., Webb, J. K., & Flambaum, V. V. 2003, MNRAS, 345, 609
 Press, W. H., Flannery, B. P., Teukolsky, S. A., & Vetterling, W. T. 1989, Numerical Recipes (Cambridge Uni. Press: Cambridge)
 Quast, R., Reimers, D., & Levshakov, S. A. 2004, A&A, 415, L7 [QRL]
 Quast, R., Baade, R., & Reimers, D. 2002, A&A, 386, 796
 Reimers, D., Baade, R., Quast, R., & Levshakov, S. A. 2003, A&A, 410, 785
 Reimers, D., Hagen, H.-J., Rodriguez-Pascual, P., & Wisotzki, L. 1998, A&A, 334, 96
 Webb, J. K., Flambaum, V. V., Churchill, C. W., Drinkwater, M. J., & Barrow, J. D. 1999, Phys. Rev. Lett. 82, 884